Soft Matter

Dynamic Article Links

Cite this: DOI: 10.1039/c2sm07058h

www.rsc.org/softmatter

PAPER

Semiflexible filament networks viewed as fluctuating beam-frames

Tianxiang Su and Prashant K. Purohit

Received 28th October 2011, Accepted 24th February 2012
DOI: 10.1039/c2sm07058h

We present a new method combining structural and statistical mechanics to study the entropic elasticity of semiflexible filament networks. We view a filament network as a frame structure and use structural mechanics to determine its static equilibrium configuration under applied loads in the first step. To account for thermal motion around this static equilibrium state, we then approximate the potential energy of the deformed frame structure up to the second order in kinematic variables and obtain a deformation-dependent stiffness matrix characterizing the flexibility of the network. Using statistical mechanics, we then evaluate the partition function, free energy and thermo-mechanical properties of the network in terms of the stiffness matrix. We show that penalty methods commonly used in finite elements to account for constraints, are applicable even when statistical and structural mechanics are combined in our method. We apply our framework to understand the expansion, shear, uniaxial tension and compression behavior of some simple filament networks. We are able to capture the stress-stiffening behavior due to filament reorientation and stretching out of thermal fluctuations, as well as the reversible stress-softening behavior due to filament buckling. Finally, we apply our method to square networks and show how their mechanical behavior is different from triangular networks with similar filament density and persistence length.

1 Introduction

Soft filamentous networks show distinct mechanical behaviors compared to conventional solids. They have a nonlinearly elastic stress-strain relation at large strains.[1–5] Also, filament gels display so-called "negative normal force" behavior: they contract under shear while usual Neo-hookean polymers expand.[6,7] Different deformation modes of the networks, such as affine *versus* non-affine modes, have been discussed in recent years.[8–11] It has also been shown that the elastic modulus of a filament network can be tuned by the density/type of the cross-linking proteins, internal motor generated stresses and by the loading frequency, *etc.*[1,3–5,12–15]

A method frequently employed to study mechanical behavior of filament networks is finite element simulation. But, typical finite element studies in this field often neglect the contribution of thermal fluctuations to the mechanics of networks, or only consider thermal effects in the undeformed configurations.[16] It is well known that at nanometer and micrometer length scales, thermal fluctuations can significantly affect the mechanical behaviors. For example, the non-linearity in the force-extension relation of the wormlike-chain model comes from stretching out thermal fluctuations at large force.[17] For a semiflexible filament network, the role of thermal fluctuations is not completely clear at present. Some recent studies found that thermal fluctuation has a noticeable influence only when the persistence length of the polymer ξ_p is comparable to the average distance between cross-links l_c,[18] while other studies suggest that thermal undulations of individual filaments are responsible for the elasticity of cross-linked network even when $l_c \ll \xi_p$.[1,19,20] Despite this uncertainty, it is commonly acknowledged that at least for low pre-strained, low density networks, configurational entropy due to thermal fluctuation plays an important role in the mechanical behavior. One of the main goals of this paper is to establish a theoretical framework that extends the finite element method such that it can account for the effect of thermal fluctuations.

Besides finite element models there are theoretical studies on networks that do include the effect of thermal fluctuations by using the wormlike-chain model, or the freely-jointed-chain model, as the constitutive law for individual filaments in the networks.[21,22] But, this may not always be appropriate because a filament in a network can be subjected to very different boundary conditions and constraints compared to an isolated filament. More importantly, the wormlike-chain model concerns only the behavior of a filament under tension. In a network, however, even under simple shear, some filaments can be subjected to significant compressive forces and bending moments.[2,23–25] The wormlike-chain constitutive law can no longer be used to describe filament mechanics in such scenarios. The method described in this paper can systematically account for the effect of thermal fluctuations instead of using the wormlike chain constitutive law locally.

Another simulation technique that has been employed to study soft networks is Brownian dynamics.[18] This method accounts for the effect of thermal motion by including the Langevin force term in the dynamic simulations.[18] The advantage of doing so is that the influence on equilibrium and dynamic properties (such as, relaxation times) of different cross-linking proteins, thermal fluctuations, pre-strain of the filaments, *etc*., can be easily investigated.[18] But, dynamic simulations are computationally costly, especially when the number of atoms/particles is large. For problems involving buckling, the results from dynamic simulations also depend strongly on the strain rate and the critical force can have significant overshoot.[26] This type of problems can be avoided in Monte-Carlo simulations of networks. The expensive step in Monte Carlo simulations is the sampling of configurations to accurately compute the ensemble averaged quantities. We note that recently improved sampling techniques have been developed and applied on filament networks.[27]

In this paper, we propose a new theoretical framework combining structural mechanics and statistical mechanics to understand the entropic elasticity of fluctuating filament networks. A filamentous network is viewed as a mechanical structure, discretized and represented by a set of generalized coordinates. In the first step, the static equilibrium state of the network under applied loads and possible constraints is determined using energy minimization (structural mechanics part). In the second step, Gaussian integrals are used to understand the fluctuation around the static state (statistical mechanics part). We approximate the local minimum energy well to quadratic order; this gives rise to a deformation-dependent stiffness matrix that characterizes the flexibility of the deformed network. We then use the stiffness matrix to calculate the partition function, from which all thermodynamic properties of the network can be determined. Our method is efficient because there is only a small extra computational cost for computing averages based on Gaussian integrals in the second step after computing the inverse of the stiffness matrix in the first step. In fact, the matrix inversion step is highly optimized in commercial finite element packages. We show that the fluctuation of the network scales linearly with the temperature and inversely with the stiffness matrix. While most previous studies have focused on homogeneous networks with one type of filament, the framework proposed in this paper can deal with heterogeneous networks easily.

We note that there exist models of rubber elasticity in the literature that view a polymer as a network of linear springs and perform a Gaussian integral to obtain the partition function (and the free energy) in terms of the determinant of a stiffness matrix.[28] But, to our knowledge, no attempt has been made to view networks of semiflexible polymers as fluctuating beam-frame structures, instead of networks of linear springs. Thinking of the network as a fluctuating beam-frame allows us to examine the effects of filament buckling which cannot be captured in a network of linear springs. Filament buckling is partially responsible for non-affine deformations and has also been shown by several studies to cause stress softening in networks.[2,16] A recent study has also proposed that buckling plays a role in organization of the networks in cells.[25] In this paper, we require our computation to follow the correct post-buckling paths and obtain the entropic elastic behavior of the networks both before and after buckling of the individual filaments.

Our focus in this paper is (1) to set up and understand the above framework, and (2) to apply the framework to simple filament networks to understand the effects of thermal fluctuations on the mechanics. We will not discuss large networks in this paper since the framework developed here can easily be incorporated into existing finite element packages to study large networks. Using finite element method to study large filament networks is feasible as many previous studies have demonstrated on systems with degrees of freedom $\sim 10^4$.[16,29–33] Our goal for this paper is to demonstrate that the proposed method can capture the entropic effects and reproduce known results on small networks, so that researchers in the community can use the finite element method to study entropic effects in networks. Although the networks in our study are simple, they capture many of the characteristic behaviors observed in experiments, such as stress-stiffening when thermal fluctuations are stretched out, stress-softening when filaments buckle and also negative normal stress when the networks are sheared.

2 Theory

2.1 Entropic elasticity of a system without constraints

The elastic energy of an individual filament in a network consists of stretching and bending energies:

$$E_{\text{elastic}} = \int_0^{L_0} \frac{K_s}{2}(\lambda - 1)^2 ds_0 + \int_0^{L_0} \frac{K_b}{2}\left(\frac{\partial \theta}{\partial s_0}\right)^2 ds_0, \tag{1}$$

where s_0 and s are the reference and deformed arc lengths, L_0 is the reference contour length before deformation, $\lambda = \partial s/\partial s_0$ and θ are the local stretch and tangent angle respectively, K_s and K_b are the stretching and bending moduli of the filament. We note that the filaments can be heterogeneous in this theory, *i.e*, K_s and K_b may vary along the filaments.

Cross-links in a polymer network (like actin-binding proteins (ABP)[34]) give rise to another energy term. Some of them constrain the angle between the cross-linked filaments[3] while others act as hinges. To model these angle constraints, we add a rotational spring, with spring constant k, at each cross-link. When there is no constraint, we set $k = 0$. The energy contributed by each of these rotational springs is:

$$E_{\text{link}} = \frac{k}{2}(\Delta\theta - \Delta\theta_0)^2, \tag{2}$$

where $\Delta\theta$ is the tangent angle difference between the cross-linked filaments and $\Delta\theta_0$ is the reference value of that angle. For example, a cross-link by macrophage ABP would have $\Delta\theta_0 = \pi/2$.[35]

The potential energy of a filamentous network also includes various force potentials due to the applied loads. For example, for a network under live hydrostatic edge tension p, the potential energy is $E_p = -pA$, with A being the current area in a 2D network. On the other hand, a shear stress τ on a filament contributes a potential energy $E_\tau = -\int \tau(\vec{r}\cdot\hat{t})ds$, with $\vec{r}$ being the position vector of the filament and $\hat{t}$ being the local unit tangent. Total potential energy of a network is $E = E_{\text{elastic}} + E_{\text{link}} + E_{\text{forcepotentials}}$.

The first step in our proposed framework is to use methods in structural mechanics to determine a static equilibrium configuration that minimizes the energy described above.† Usually, the

† The theory described here is not restricted to filament networks alone. Other types of energies may be included if a different fluctuating mechanical structure, such as a nano shell, is under investigation.

ART ■ C2SM07058H

structure is discretized into elements and becomes a system with finite degrees of freedom (dof) characterized by a set of generalized coordinates q_i ($i \in [1,\text{dof}]$). In our method, each filament in the network is discretized into small segments whose lengths are much smaller than the persistence length. The generalized coordinates are the local stretches λ_i and local tangent angles θ_i for each segment. Energy minimization is performed on the discrete structure using Newton's method, which involves the computation of the current stiffness matrix $\mathbf{K}_q$: $[\mathbf{K}_q]_{ij} = \partial^2 E/\partial q_i \partial q_j$. This matrix is evaluated at the current configuration under given applied loads, so that geometric non-linearity is taken into account. Using the current stiffness matrix is crucial when buckling and post-buckling behaviors are under investigation. Below, we will denote the minimum energy configuration as $\vec{q}_{\min}$. A 'static' result mentioned later in this paper will refer to the solution *without* taking thermal fluctuations into account.

The next step is to apply statistical mechanics to study the entropic elasticity behavior around the static solution. We denote the fluctuation away from the static state as $\Delta\vec{q} = \vec{q} - \vec{q}_{\min}$, and approximate the energy of the states around the static state up to the second order:

$$E = E_{\min} + \frac{1}{2}\Delta\vec{q}^{T}\cdot\mathbf{K}_q\Delta\vec{q}, \tag{3}$$

with $E_{\min}$ being the energy of the static state. We emphasize that $\mathbf{K}_q$ is the current stiffness matrix. It depends on the current static state and varies as one changes the applied loads. The partition function of such a system is a multidimensional Gaussian integral and it is given analytically by:[36,37]

$$Z = \int \exp\left(-\frac{E}{k_B T}\right) d\vec{q} = e^{-\beta E_{\min}}\sqrt{\frac{(\pi k_B T)^{\text{dof}}}{\det\mathbf{K}_q}}, \tag{4}$$

with $\beta = 1/k_B T$, k_B being the Boltzmann constant and T being the absolute temperature. The free energy of the system, neglecting a constant term, is:

$$G = -k_B T\ \log Z = E_{\min} + \frac{Tk_B}{2}\log\left(\det\mathbf{K}_q\right). \tag{5}$$

A more important result relates to the fluctuations of the independent coordinates, and it can be obtained by doing the Boltzmann weighted average:

$$\left\langle \Delta q_i \Delta q_j \right\rangle = \frac{1}{Z}\int\left(\Delta q_i \Delta q_j\right)\ \exp(-\beta E) d\Delta\vec{q} = k_B T[\mathbf{K}_q^{-1}]_{ij}. \tag{6}$$

This result tells us that thermal fluctuation of the independent variables is determined by (1) thermal energy $k_B T$, and (2) inverse of the current stiffness matrix. For a system on the length scale of *nm* and force scale of *pN*, the stiffness is usually comparable to $k_B T$ at room temperature. Therefore, thermal fluctuations of such nano-scale systems are significant and must be taken into account. We note that eqn (6) is a natural generalization of the equipartition theorem. To see this, we recall that the equipartition theorem for a one-dof linear system reads $\frac{1}{2}k\langle q^2\rangle = \frac{1}{2}k_B T$, which gives $\langle q^2\rangle = k_B T/k$.

The thermal average of other quantities, say $A = A(\vec{q})$, can be determined using a Taylor series expansion:

$$\langle A(\vec{q})\rangle = \left\langle A(\vec{q}_{\min}) + \frac{\partial A}{\partial q_i}\Delta q_i + \frac{1}{2}\frac{\partial^2 A}{\partial q_i \partial q_j}\Delta q_i \Delta q_j \right\rangle \tag{7}$$

$$\langle A(\vec{q})\rangle = A(\vec{q}_{\min}) + \frac{k_B T}{2}\frac{\partial^2 A}{\partial q_i \partial q_j}[\mathbf{K}_q^{-1}]_{ij}. \tag{8}$$

We see that the thermal average of a quantity $\langle A\rangle$ is, in general, different from the static value $A(\vec{q}_{\min})$ determined by energy minimization, as long as $\partial^2 A/\partial q_i \partial q_j \neq 0$. Note that if the quantity A is the energy E, then $\partial^2 E/\partial q_i \partial q_j = [\mathbf{K}_q]_{ij}$, and eqn (8) reduces to $\langle E\rangle = \frac{1}{2}\cdot\text{dof}\cdot k_B T$, which is the equipartition theorem. When we apply the theory to study a network in the following sections, the quantity A can be the area of the network, or the position of a node, or the angle between two filaments.

2.2 Including constraints in the system

In the previous section, we discussed the theoretical framework in which no constraints are posed on the independent coordinates $\vec{q}$. However, spatial constraints are commonly met. For example, a filament with two ends clamped has a constraint that the tangent angles at the ends are zero and not free to fluctuate. Similarly, a displacement boundary condition poses a constraint on the gerneralized coordinates. In this section, we discuss methods to deal with such constraints.

In finite elements, the penalty method is commonly used to enforce spatial constraints. This method replaces the rigid spatial constraints by very stiff springs. We shall see below that similar ideas can be used even in statistical mechanics. Suppose a spatial constraint on $\vec{q}$ can be expressed as $g(\vec{q}) = 0$. The partition sum must then be evaluated over the allowed configurations that satisfy $g = 0$:

$$Z = \int \exp\left(-\frac{E}{k_B T}\right)\delta(g) d\vec{q}. \tag{9}$$

To deal with the additional Dirac delta function in eqn (9), we use the expression $\delta(g) = \lim_{k\to\infty}\sqrt{k/\pi}\, e^{-k g^2}$ which turns the expression for the partition function into:

$$Z = \lim_{k\to+\infty}\sqrt{\frac{\beta k}{\pi}}\int \exp\left(-\frac{E + kg^2}{k_B T}\right) d\vec{q}. \tag{10}$$

Now, in the limit as $k \to +\infty$, the partition function has exactly the same form as the one without spatial constraints if an effective energy $E_{\text{effective}} = E + kg^2$ is used for the structure. This is essentially the same idea as the penalty method. We replace the constraints (removing the delta function) with stiff springs (adding large penalty energy to the system). When we do the computation, we do not take k as infinity. Instead, we just ensure $k_B T/k$ is very small so that there are negligible fluctuations in the constrained degree of freedom.

Another way of dealing with the delta function is to use its Fourier transform which again can change the constrained system into one without constraints.[36,37] But, if we use the Fourier transform, we have to change the integration path on the complex plane to evaluate the partition function, and the effective energy has a complex value. Moreover, in the Fourier transform method, each constraint adds one more degree of

ART ■ C2SM07058H

freedom to the structure. This is not favorable since it requires more computational effort in manipulating the stiffness matrix. For these reasons we will use the penalty method to enforce spatial constraints.

The advantage of the proposed theoretical framework is that it can be applied to evaluate the entropic elasticity and thermal fluctuations of any mechanical structure, including frame structures, plates, shells or membranes. Using finite elements to study these systems is now standard, especially with many commercial finite element packages being available. We have shown here that adding the effects of thermal fluctuation to the structural mechanics requires simply the inverse of the stiffness matrix, which is typically already available from the finite element calculation.

To test our theory, we first apply the framework described above to the extension of a single filament. The thermal average of the end-to-end extension of the filament is computed under different tensile loadings. As expected, this thermal average is less than the static extension because fluctuations tend to shrink the end-to-end distance of the filament. The result (Fig. 1) from our computation matches exactly with the known analytic solution for an extensible wormlike chain (2D):[37,38]

$$\langle x \rangle = L + \frac{FL}{K_s} - \frac{k_B T L}{4\sqrt{K_b F}}\left[\coth\left(L\sqrt{\frac{F}{K_b}}\right) - \frac{1}{L}\sqrt{\frac{K_b}{F}}\right], \quad (11)$$

where $\langle x \rangle$ is the average end-to-end extension of the chain under applied force F, and L,K_b,K_s are respectively the contour length, bending and stretching moduli of the chain. This result verifies the proposed framework and our computation scheme. In fact, the framework has been successfully applied to study an isolated fluctuating heterogeneous chain under end-to-end loads,[37] under general distributed loads,[39] and under confinement.[40] We will next apply our framework to simple 2D filament networks.

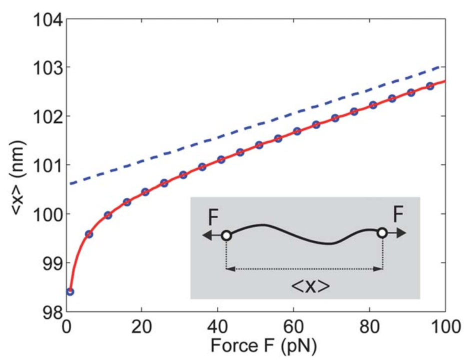

Fig. 1 Force-extension relation for an isolated hinged-hinged filament. Blue dashed line: static computational results without thermal fluctuation. Blue circles: computational results with thermal fluctuation using eqn (8). Red line: known analytic solution for an extensible wormlike chain shown in eqn (11). The filament with contour length 100.58 nm is discretized into n = 100 segments in the computation. Stretching and bending moduli are K_s = 1000k_BT/nm and K_b = 250$k_BT \cdot$ nm respectively.

3 Results and discussions

3.1 Hydrostatic edge tension on a triangular network

We first consider the expansion of a single hexagon formed by cross-linking semiflexible filaments together. Fig. 2A shows its reference and deformed static configurations under hydrostatic tension. The ratio between the contour and persistence length of each filament is $L/\xi_p = 2$. The stretching modulus is $K_s = 10k_BT$/nm. The filaments are cross-linked without angle constraints. Under live stepwise-increasing edge load p, the hexagon expands. The area of the hexagon, with and without thermal fluctuations, is calculated using eqn (8), and the results are shown in Fig. 2B. When thermal fluctuation is taken into account, the hexagon stiffens as it expands, with the 2D bulk modulus (or area expansion modulus) increasing from K_{bulk} = 0.07 pN nm^{-1} to 1.29 pN nm^{-1}. This is because at the initial stage of expansion, the deformation is caused by stretching out thermal fluctuations (easy), instead of elastically stretching the filaments (difficult).

The computational results in Fig. 2B, both with and without thermal fluctuations, can be verified by an analytic one-dof model described below. Let us imagine a toy filament network model shown in the inset of Fig. 2B. n cross-linked filaments are oriented uniformly like the spokes of a wheel, bounded by a circular filament of radius r_0 in its reference state. Under edge tension, the radius of the circular filament increases to r, and the interior n filaments are stretched. We denote by $w(r)$ the energy density function for each filament; then under hydrostatic edge tension, the potential energy of the toy network is $E(r) = 2r(\pi + n)w(r) - p\pi r^2$. Energy minimization ($\partial E/\partial r = 0$) leads to a relation between the radius r and edge tension p:

$$\left(1 + \frac{n}{\pi}\right)\frac{F(r)}{r} = p, \quad (12)$$

where $F(r)$ is the force extension relation for a single filament. Surprisingly, eqn (12) matches with our computational results, *both with and without thermal fluctuations*. In particular, if we choose a static linear force-extension relation $F(r) = K_s(r/r_0 - 1)$ in eqn (12), it reproduces our computational results without thermal fluctuations. The analytic static r–p relation turns out to be

$$r = \frac{r_0}{1 - pr_0/K_{\text{eff}}}, \quad (13)$$

with $K_{\text{eff}} = (1 + n/\pi)K_s$ being an effective stiffness. This suggests that the static bulk modulus depends linearly on the filament density $\rho_0 = n/(\pi r_0^2)$ inside the network. More importantly, from eqn (13), we obtain a static bulk modulus that varies as r^{-1}, which suggests a strain softening effect, as opposed to strain stiffening when thermal fluctuations are accounted for. This highlights the importance of considering thermal fluctuations in discussing the mechanics of a network. Furthermore, if we choose the extensible wormlike-chain model given by eqn (11) for $F(r)$ in eqn (12), the computational result with thermal fluctuations is reproduced (Fig. 2B). The match between the computational results and the analytic one-dof toy model verifies our proposed method. But, it is important to note that a simple analytic model works because no buckling or angle constraint is involved in this example.

A transition from entropic expansion, where thermal fluctuations play a significant role, to enthalpic expansion is expected as

ART ■ C2SM07058H

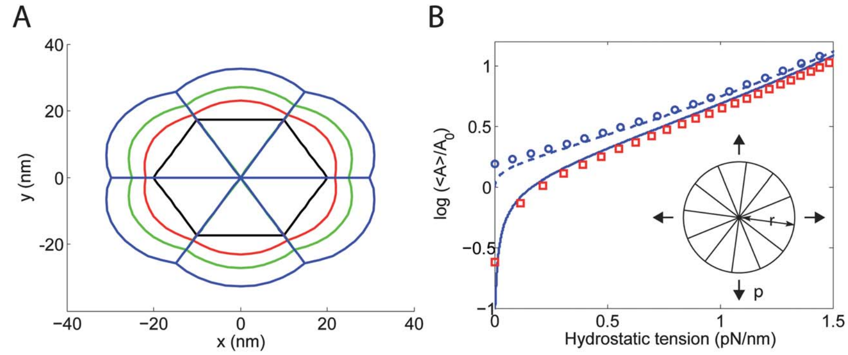

Fig. 2 Expansion of a hexagon. (A) Static reference (black) and deformed configurations under hydrostatic tension. The ratio of contour length to persistence length for each filament is 2 : 1. (B) Area of the hexagon *versus* edge tension p. Dashed line is the static computational result without thermal fluctuations, while the solid line is the result with thermal fluctuations, which shows 'strain stiffening' with bulk modulus increasing from $K_{\mathrm{bulk}} = 0.07$ pN nm^{-1} to $K_{\mathrm{bulk}} = 1.29$ pN nm^{-1}. Circles and squares are the results from an analytic toy model shown in the inset, which agree well with our computational results. The area A is nondimensionalized by A_0, the reference area of the network.

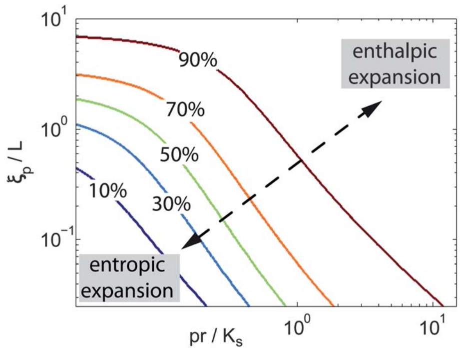

Fig. 3 Transition from entropic to enthalpic expansion. Contours of $K_{\mathrm{bulk,thermal}}/K_{\mathrm{bulk,static}}$ are plotted on the $\xi_p - p$ plane. Both the persistence length ξ_p and the edge tension p have been nondimensionalized. Small persistence length or edge tension leads to small $K_{\mathrm{bulk,thermal}}/K_{\mathrm{bulk,static}}$, meaning entropic contribution is significant. Increasing persistence length or the edge tension reduces the contribution from thermal fluctuations.

one increases the edge tension p, or the persistence length ξ_p, since both of these reduce fluctuations. In fact, a similar transition in shear[8–10] has been reported as a result of changing the cross-link density and filament concentration to suppress fluctuations. To illustrate such a transition, we calculate the tangent bulk modulus $K_{\mathrm{bulk}} = Adp/dA$, with and without thermal fluctuations, and make a contour plot of their ratio $\alpha = K_{\mathrm{bulk,thermal}}/K_{\mathrm{bulk,static}}$ on the $\xi_p - p$ plane. In the small ξ_p and small p regime, we get a small $\alpha \ll 1$, which suggests a significant softening of the network by thermal fluctuations. On the other hand, in the large ξ_p and large p regime, $\alpha \rightarrow 1$, which suggests enthalpic stretching dominates. The contour plot is shown in Fig. 3.

We also report, using our computations, that changing the bending modulus of filaments only affects the plots with thermal fluctuations, while changing the stretching modulus affects both the static and thermal results (Fig. 4A–B). This is confirmed by the analytic expressions of the one-dof toy model. In Fig. 4C, we show that adding filaments in the hexagon stiffens the structure, while removing filaments softens it. This confirms that our method qualitatively captures the result that the entropic elasticity of a network can be tuned by changing the filament density.

3.2 Simple shear on a triangular network

In this section, we study shear deformation by applying uniform shear stresses on the top and bottom filaments of the hexagon

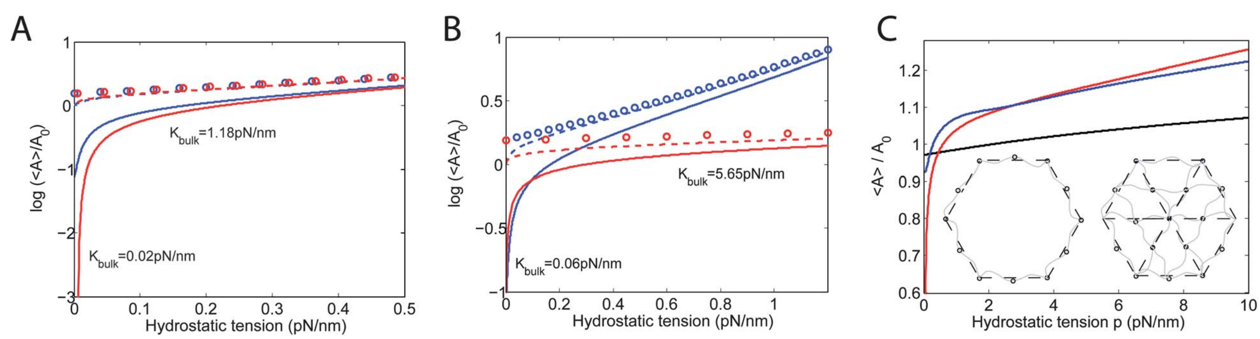

Fig. 4 Effects of changing the (A) bending, (B) stretching moduli and (C) filament density and connectivity on the expansion behavior of a hexagon. The results in Fig. 2B are superimposed as blue lines and blue circles for comparison. (A) Reducing the persistence length (red: $L/\xi_p = 4$, blue: $L/\xi_p = 2$) only affects the result with thermal fluctuations. (B) Increasing the stretching modulus to $K_s = 100k_BT$/nm (red) affects both the static and thermal results. (C) Expansion behavior of hexagons with different filament densities and connectivities. Red line is the result for an empty hexagon (inset). Black line is the result for a hexagon with higher filament density (inset).

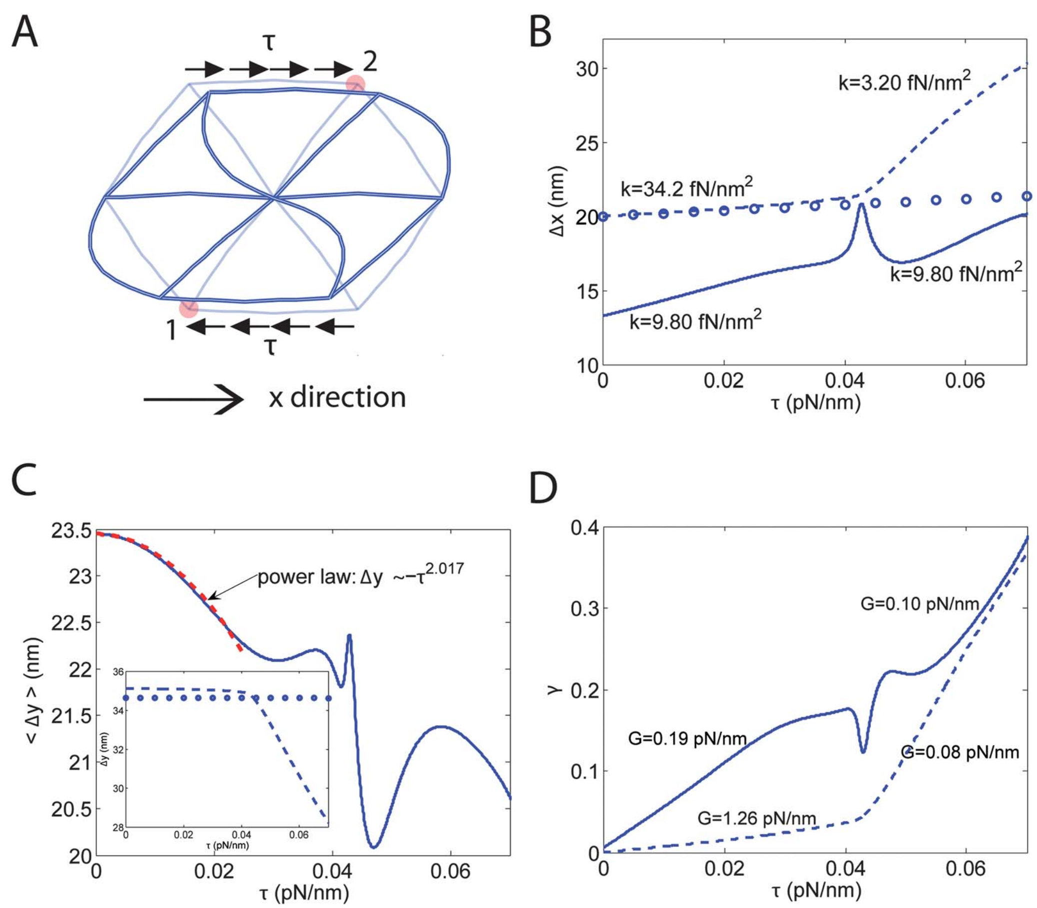

Fig. 5 Shear on a triangular network. (A) Uniform distributed forces in $\pm x$ direction are applied on the top and bottom filaments of hexagon to cause the shear deformation. (B) Δx is the distance, in X direction, between node 1 and node 2 shown in A. It is plotted as a function of τ. Effective stiffness is defined as $k = d\tau/d(\Delta x)$ here. Dashed line is the result without thermal fluctuation. Solid line is the result with thermal fluctuations. Circles are the results from the analytic static solutions assuming affine deformation (eqn (15)). They match with our computational results at small τ. For large τ, buckling occurs and the deformation of the hexagon is non-affine. (C) Height of the hexagon during shear. Static result without thermal fluctuations is shown in inset. (D) Shear strain γ as a function of the shear stress τ. Effective shear modulus can be defined as $G = d\tau/d\gamma$. Dashed line: static solution. Solid line: result including the thermal effects. The stress-strain relation is linear before and after buckling at $\tau \approx 40$ fN nm^{-1}. For the static solution, the shear modulus decreases significantly after buckling. For the result that includes thermal fluctuation, the shear modulus decreases after buckling but the change is not as large as in the static case.

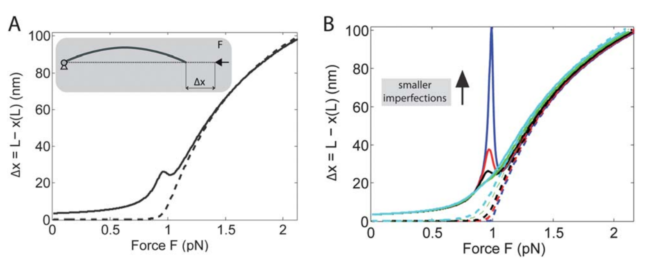

Fig. 6 Axial shortening *versus* compressive force for a hinged-hinged filament shown in (A) inset. (A) Dashed line: computational result without thermal fluctuation. Solid line: result with thermal fluctuation. Small imperfections are introduced to the initial straight configuration of the filament. (B) Influence of the initial imperfection. The peak around the buckling point becomes taller and sharper as we reduce the imperfection. The fluctuation peak can be an artifact of the second order expansion in our theory. But, we show in Fig. 7 that even for a quartic system, one still expects large fluctuations at the point where the second order term vanishes.

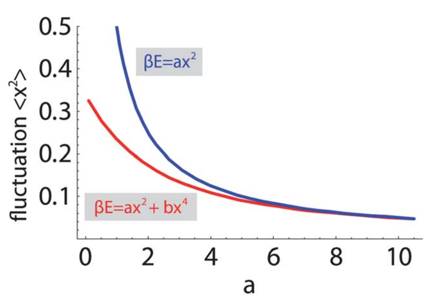

Fig. 7 Thermal fluctuations, $\langle x^2\rangle = Z^{-1}\int x^2\exp(-\beta E)dx$, of a one-dof system with quartic energy $\beta E = ax^2 + bx^4$ (red) and quadratic energy $\beta E = ax^2$ (blue). $\langle x^2\rangle$ increases but remains finite as $a \rightarrow 0$ when the quartic term is non-zero. For large enough values of a, the quadratic term is sufficient to account for the fluctuations.

(Fig. 5A). Compared with the expansion process, the challenge of considering shear is that some filaments in the network are under compression and will buckle, which has been shown in

ART ■ C2SM07058H

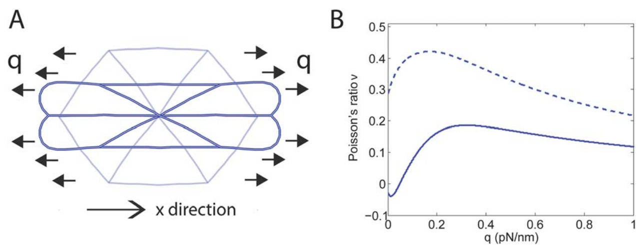

Fig. 8 Uniaxial deformation of a hexagon. (A) Static reference and deformed configurations. (B) Poisson's ratio as a function of the tension force q. The dashed line is the static result without thermal fluctuations. At $q = 0$, $\nu = 1/3$, as predicted using an analytic toy model. The solid line is the computational result with thermal fluctuations. Interestingly, the Poisson's ratio is negative near $q = 0$ when thermal fluctuation is included.

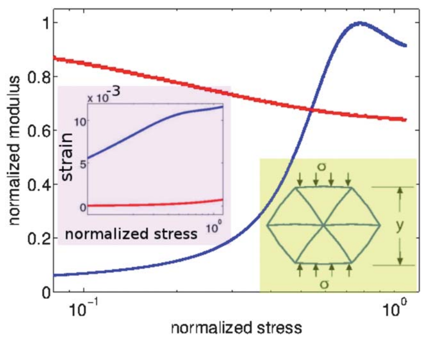

Fig. 9 Stress softening due to buckling. We compress a triangular network (a hexagon here, shown in inset) and measure its modulus as a function of the compressive stress. Blue and red lines are the results with and without thermal fluctuations respectively. With thermal fluctuations, the network shows stress stiffening at the beginning due to stretching out of thermal fluctuations. This is followed by stress softening because of buckling of filaments. The same phenomenon is observed in experiments on actin networks (Fig. 3 in Chaudhuri *et al.*[2]). Note that as in Chaudhuri *et al.*,[2] the stress on the x axis is shown on a log scale. The stress-strain curves with (blue) and without (red) thermal fluctuations are shown as inset. Here we use the parameters for a actin filament network: $\xi_p = 10$ μm, $L = 5$ μm.

experiments to play a crucial role in determining the mechanics of a network.[2,16,41] But, the *static* behavior *before* buckling can still be understood using a simple two-dof analytic model, the results of which can serve to verify our computational results and also shed some light on the problem. We will first briefly discuss this analytic model and then apply our method to understand the shear behavior with buckling.

The analytic two-dof model is set up as follows. Suppose the hexagon under shear (shear stress τ is applied on the top and bottom filaments) suffers affine deformation with deformation gradient:

$$\mathbf{F} = \begin{bmatrix} 1 & F_{12} \\ 0 & F_{22} \end{bmatrix}. \tag{14}$$

We evaluate the potential energy E (elastic energy for each filament plus force potential energy due to the applied shear stress τ) of the hexagon under such a deformation and perform energy minimization $\partial E/\partial F_{ij} = 0$ to find F_{12} and F_{22}. An analytic solution exists and the result is:

$$F_{12} = \frac{4}{\sqrt{3}}\frac{\bar{\tau}}{(1-\bar{\tau}^2)^2}, F_{22}^2 = \frac{4}{3(1-\bar{\tau})^2} - \frac{1}{3}\left[1 + \frac{4\bar{\tau}}{(1-\bar{\tau}^2)^2}\right]^2, \tag{15}$$

with $\bar{\tau} = \tau L_0/2K_s$ being a dimensionless shear stress. Here L_0 is the contour length of the individual filaments. In the small shear stress limit $\bar{\tau} \ll 1$, the solution is approximately:

$$F_{12} \approx \frac{4}{\sqrt{3}}\bar{\tau}, F_{22} \approx 1 - \frac{2}{3}\bar{\tau}^2. \tag{16}$$

The fact that $F_{22} \leq 1$ shows that a hexagon will contract in the y direction under shear, even in the *absence* of thermal fluctuations. This is consistent with previous studies that showed athermal networks very generally exhibit negative normal stress.[11] Also, eqn (16) leads to an analytic static shear modulus of $G = \sqrt{3}K_s/2L_0$ for the hexagon. We note that the same analysis can be applied to an empty hexagon without the interior filaments. Interestingly, the results of eqn (15) remain the same, except that the dimensionless $\bar{\tau}$ has to be redefined as $\bar{\tau} = \tau L_0/K_s$. The static shear modulus is half of that for a regular hexagon with the interior filaments. Though simple and analytic, this model cannot be extended to include the contribution of thermal

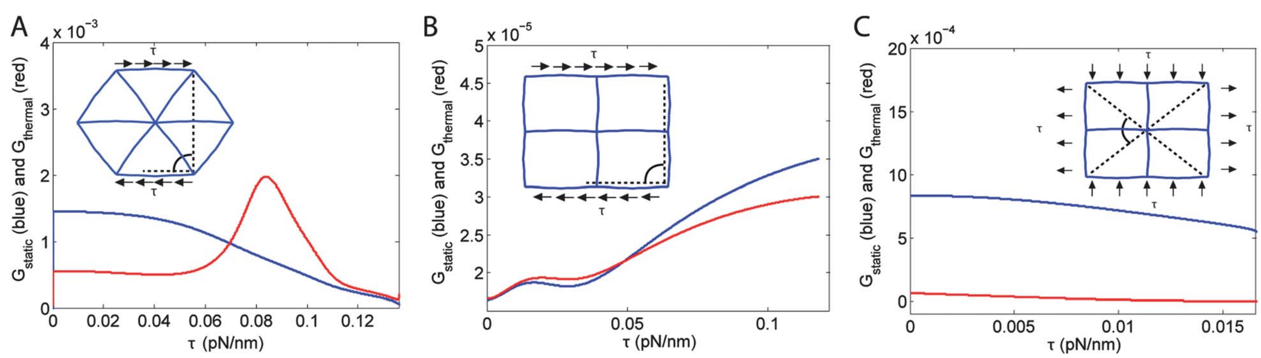

Fig. 10 Tangent shear modulus G *versus* shear stress τ for (A) a triangular network and (B,C) a square network. Blue lines and red lines are the result with and without thermal fluctuations respectively. A comparison between the three figures shows that a triangular network has much higher shear modulus than a square network. Rotational springs are present at each cross-link with stiffness $k = 1k_BT$ and the lengths and stiffness of the filaments are the same for the triangular and square networks. Shear strain is measured as the change of angle between the dashed lines shown in the figures.

ART ■ C2SM07058H

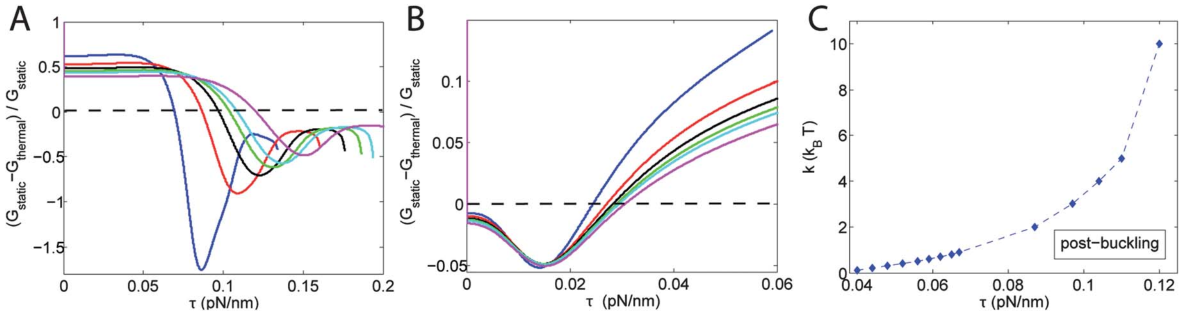

Fig. 11 Shear of (A) hexagons and (B) squares with different rotational stiffness at the cross-links. Shear stress is applied in a manner shown in insets of Fig. 10A and B. At a given shear stress τ, the tangent shear moduli G_{static} and G_{thermal} are calculated. Plots (A) and (B) show their difference, normalized by G_{static}, against the shear stress. At each cross-link of the networks, there is a rotational spring with stiffness k. Blue, red, black, green, cyan and magenta lines are for $k = 1,2,3,4,5$ and $10k_BT$ respectively. Plot (C) shows the buckling shear stress τ for hexagons with different rotational spring constant k.

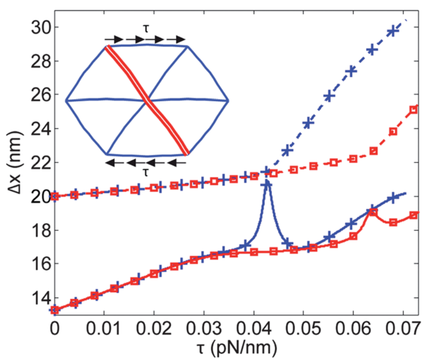

Fig. 12 Shear of a heterogeneous hexagon in which one diagonal filament (shown in thicker stroke in the inset) has 1.75 times the persistence length of the rest of the filaments. x-direction separation Δx, between the top and bottom filaments as a function of the shear stress τ is shown. Red □ solid and dashed lines are the results with and without thermal fluctuations respectively. As a comparison, the behavior of a homogeneous hexagon is shown in blue + lines. Replacing the diagonal filament with a stiffer filament affects the behavior of the hexagon significantly only after buckling occurs. The stiff impurity shifts the buckling event to a larger load and also suppresses the fluctuation peak. This effect is seen for persistence length ratios other than 1.75 (results not shown).

fluctuations. The wormlike-chain model cannot be used for the filaments under compression, not to mention the buckling behavior that is neglected at large τ.

We can still apply our method of combining structural and statistical mechanics to this problem. But, before using it on the triangular network, we will first study the compression of an isolated filament with both ends hinged (Fig. 6A inset). This will help us understand the effects of thermal fluctuations on buckling. We use eqn (8) to obtain the relation between the compressive force F and the axial shortening $\langle \Delta x \rangle$ of the filament. The results, both with and without thermal fluctuations, are shown in Fig. 6A. The result *without* thermal fluctuation is classical, with Δx increasing dramatically after buckling.[42] The result *with* thermal fluctuation, on the other hand, is more interesting. A peak appears at the buckling load, suggesting large thermal fluctuations caused by a loss of stability when buckling occurs. This is an artifact of the second order expansion in our theory. We will discuss this again later. After transition to the post-buckling path (we verify that the Euler elastica is correctly obtained), however, the filament regains stability and thermal fluctuation is reduced. Before buckling, thermal fluctuation causes the end-to-end distance of the filament to be less than the static value, but at large compressive force the opposite is true. This result agrees with a previous study on the role of thermal fluctuation on a buckled rod.[43]

To obtain the correct post-buckling behavior (the Euler elastica) in the above study, we introduced small imperfections into the initial straight configuration of the filament.[42] The reasons for doing so are as follows. (1) With small imperfection, the computational result in the structural mechanics part naturally follows the correct stable post-buckling path,[42] otherwise, it is possible that the computational result goes to the unstable local energy maximum after buckling. (2) Introducing small imperfections into the initial configuration avoids the singularity of the stiffness matrix at the buckling load.[42] Singularity of the stiffness matrix is not desirable, since the partition function is determined by $(\det \mathbf{K}_q)^{-1}$ and the fluctuations are determined by $\mathbf{K}_q^{-1}$. (3) Real filaments in gels are always thermally fluctuating. Therefore, they are never compressed with an initial straight configuration. Compression with initial imperfection is a better model to describe fluctuating filaments and has been used in simulations of networks.[16] We point out that the peak in Fig. 6A depends strongly on the amount of imperfection in the initial configuration (Fig. 6B). For small imperfection, the path is closer to the singularity so the peak is large. For large imperfection, on the other hand, the transition is smoother and the peak is smaller. For fluctuating filaments, we expect the initial configurations to be bent so that the overall response would look smooth.

It is worth discussing the quadratic approximation of the energy (eqn (3)) around the buckling point. This approximation is appropriate before and after buckling, since the structure is stable in those regimes and the leading order of the energy is the second order. Near the buckling load, especially when imperfections are small, the second order term in energy may become very small and the leading order may be quartic. The fluctuation peak in Fig. 6 is an artifact of our second order expansion.[43–45] But, one still expects large thermal fluctuations around the buckling load even if the quartic term is included in the calculations. In fact, for a one-dof system with energy $E(x) = ax^2 +$

ART ■ C2SM07058H

bx^4, both the partition function and the fluctuations $\langle x^2 \rangle$ can be evaluated analytically. The expressions involve Bessel functions and are not shown here. In Fig. 7, we plot $\langle x^2 \rangle$ as a function of a for a fixed b. We see an increase in the fluctuations $\langle x^2 \rangle$ for this quartic system as the quadratic term vanishes. We note that the error in neglecting the quartic term around the buckling point will not affect our computational results after buckling occurs.

Now that we understand the buckling of a single filament with thermal fluctuation, we return to shear of a triangular network. Again, the stretching modulus is $K_s = 10k_BT$/nm and L/ξ_p is set to 2 so that the filaments are semiflexible. Fig. 5A shows the static reference and deformed configurations obtained in our computations. To avoid the singularity, we again start with initial curved configurations with small imperfection. Some filaments buckle at large shear force, as expected. Using eqn (8), we calculate the separation between the top and bottom filaments in the x direction, denoted as Δx, as a function of the applied shear stress τ. Both the results with and without thermal fluctuations are shown in Fig. 5B. For the results *without* thermal fluctuations, our computation almost exactly matches with the toy analytic affine model (eqn (13)) upto the buckling load $\tau \approx 0.04$ pN nm^{-1}. As expected, however, the toy model fails to capture the post-buckling behavior because of the affine deformation assumption. Our computational results, on the other hand, capture the buckling events and show that buckling significantly softens the hexagon and makes it much more deformable in the post-buckling regime. In fact, our result shows that a stiffness defined as $k = d\tau/d(\Delta x)$ decreases from 34.2 fN nm^{-2} before buckling to 3.20 fN nm^{-2} after buckling. These are the results without thermal fluctuations, and they show the importance of *not* making the affine assumption when buckling is involved. For the results with thermal fluctuations, we obtain a much smaller initial stiffness $k = d\tau/d(\Delta x) = 9.80$ fN nm^{-2} compared to the static value. This is a consequence of stretching out thermal fluctuations in the initial state. Moreover, while the static solution suggests that the hexagon softens after buckling, the results with thermal fluctuations suggest the opposite. We obtain an increase, though not significant, in the stiffness k after buckling when fluctuations are included. We also note, as in the case of compression of an isolated filament, that the peak in the thermal results in Fig. 5B implies we are near an instability (.We checked the axial force of each of the filaments in the network as a function of the shear stress and confirmed that the peak corresponds exactly to the buckling event).

Changing the bending modulus of the filaments has a significant effect on the thermal solution. In particular, decreasing the persistence length from $L/\xi_p = 2$ to $L/\xi_p = 4$ (L is the filament contour length) reduces the initial stiffness $k = d\tau/d(\Delta x)$ to only 3.30 fN nm^{-2} before buckling occurs. This is expected, since filaments with smaller persistence length have more thermal fluctuations and therefore are easier to shear. Buckling occurs earlier, which is also expected.

We now turn to the deformation of the hexagon in the y direction. We calculate the height of the hexagon, denoted as Δy, as a function of the shear stress. The computational results, with and without thermal fluctuation, confirm that the hexagon indeed contracts during shear (Fig. 5C). Before buckling, the contraction Δy (including thermal fluctuations) scales as $\Delta y \sim -\tau^{2.017}$, which suggests that the separation in the y direction decreases quadratically in the initial stages. Further, shear strain of the hexagon can be defined as $\gamma = \Delta x/\Delta y$, with Δx and Δy discussed above.‡ We show the relation between γ and τ in Fig. 5D. An effective tangent shear modulus can be introduced as $G = d\tau/d\gamma$. For the static solution, the shear modulus is significantly reduced (from $G = 1.26$ pN nm^{-1} to $G = 0.08$ pN nm^{-1}) after buckling. The static initial shear modulus agrees well with the analytic value of the simple affine toy model. For the results that include thermal fluctuations, the shear modulus does not change a lot. The modulus before buckling is due to stretching out thermal fluctuations, while the modulus after buckling is due to elastic stretching.

3.3 Uniaxial tension on a triangular network

We also apply tensile stress q on the hexagon to study its uniaxial deformation (Fig. 8A). As in the previous section, an affine toy model can be set up. In particular, two components of the deformation gradient vanish $F_{12} = F_{21} = 0$ while the other two, F_{11} and F_{22}, are left as unknowns to minimize the static potential energy. The results are $F_{11} = 1 + 3ql_0/K_s$ and $F_{22} = 4/3 - (1 + 3ql_0/K_s)^2/3$. The initial Poisson's ratio is predicted as $\nu = 1/3$ for the hexagon. Our static computational result confirms this value (Fig. 8B), but, the result with thermal fluctuations is quite different (Fig. 8B). Curiously, we find that the Poisson's ratio of a hexagon is negative near $q = 0$ when thermal fluctuations are included.

We have now illustrated our method with triangluar networks that are known to be isotropic.[46] In the remainder of the paper, we will discuss some other applications of our method.

3.4 Applications

3.4.1 Strain softening due to filament buckling. Actin networks have been shown to undergo strain stiffening followed by strain softening under compression.[2] The initial strain stiffening is due to stretching out of thermal fluctuations while the softening effect is suspected to result from buckling of actin filaments, because the stress-strain relation is reversible when the compressive load is released.[2] Here we use the parameters of a actin filament network ($\xi_p = 10$ μm, $L = 5$ μm) and compress a single hexagon as performed in the experiment[2] (Fig. 9 inset). The stress-strain relation is calculated (Fig. 9 inset), from which the elastic modulus as a function of stress is determined. The result is shown in Fig. 9 (blue line). This plot qualitatively agrees with the experimental measurement shown in Fig. 3 in Chaudhuri *et al.*[2] As in the experiment, we observe an initial strain stiffening due to entropic effects, followed by strain softening due to buckling of filaments. This is the result with thermal fluctuations taken into account. We note that since the network is 2D in our calculation, we cannot compare the modulus directly with that measured in the experiment. If thermal fluctuation is turned off (Fig. 9 red line), no initial strain stiffening is observed in our calculations.

3.4.2 Square networks, angle constraints. In the examples discussed so far, we assumed that the cross-links are all hinges.

‡ To be exact, Δx here is the Δx shown in Fig. 5B minus L_0.

ART ■ C2SM07058H

But, some cross-links in real networks put constraints on the angle between the linked filaments. In fact, cross-links in a square network must have rotational stiffness in order for the network to resist shear. In the examples below, we add rotational springs (spring constant $k = 1k_BT$) to the cross-links and compare the behavior of a triangular network with a square network under shear (Fig.. 10). Filaments in both networks have the same contour length, stretching and bending moduli. For both networks the tangent shear modulus $G = d\tau/d\gamma$ is calculated as a function of the shear stress τ. In particular, since a square network has two shear moduli,[47] we perform two shear tests in different directions on the square (Fig. 10B–C). The computational results are shown in Fig. 10. The shear modulus of a triangular network, with or without thermal fluctuations, is much higher than those of a square network with filaments of the same length and mechanical properties. We also compute ΔG, the difference between the static shear modulus and the shear modulus with thermal fluctuations, as a function of the shear stress τ (Fig. 11, A for a triangular network and B for a square network sheared as shown in inset of Fig. 10B). For a triangular network, ΔG is initially positive and changes to negative after buckling, while for a square network, the trend is exactly the opposite. Fig. 11C shows a phase diagram that separates the pre-buckling and post-buckling regimes for a triangular network with different rotational spring stiffness.

3.4.3 Heterogeneous networks. Many cellular networks are not homogeneous. They consist of a complex scaffold of several distinct filaments with different mechanical properties. In fact, it has been proposed that the compressive load in the cytoskeleton is borne by microtubules, whose persistence length is about 2 orders of magnitude larger than actin filaments.[3] For this reason, it is important to study heterogeneous networks and several recent studies have looked into the effects of incorporating microtubules on the mechanics of actin networks, and numerically investigated two-component networks of biopolymers.[30,48,49] Our framework can deal with heterogeneous networks easily. As an example, we increase the bending modulus of one diagonal filament in the previously studied hexagon to construct a heterogeneous network (Fig. 12 inset) and redo the shear test. Interestingly, the behavior of the hexagon is not affected by such a replacement before buckling. Our computational results show that the stiff impurity shifts the buckling event to a larger load and also suppresses the peak in the solution that includes the effect of thermal fluctuations (Fig. 12).

4 Conclusions

In this paper a combination of structural and statistical mechanics is used to investigate the entropic elasticity of filamentous networks. The structural mechanics part of the theory is standard, involving discretizing a structure followed by energy minimization. The statistical mechanical part, on the other hand, involves an approximation of the energy upto quadratic order, which in turn makes it possible to compute the partition function as a Gaussian integral. The free energy and other thermodynamic quantities are obtained using the partition function or the Boltzmann weighted ensemble averages. This framework is applied only to simple networks here and its ability to capture various mechanical behaviors seen in experiments is demonstrated. The importance of including thermal fluctuations and the effects of filament buckling are discussed. With the framework demonstrated, we hope that researchers will move on to using available finite element packages to study larger 3D filament networks and other mechanical structures (such as membranes) for which thermal fluctuations play a significant part in the physics.

Acknowledgements

We acknowledge partial support to PKP through an NSF CAREER award grant number NSF CMMI-0953548.

References

1 M. L. Gardel, J. H. Shin, F. C. MacKintosh, L. Mahadevan, P. Matsudaira and D. A. Weitz, Elastic behavior of cross-linking and bundled actin networks, *Science*, 2004, **304**(5675), 1301–1305.
2 O. Chaudhuri, S. H. Parekh and D. A. Fletcher, Reversible stress softening of actin networks, *Nature*, 2007, **445**(7125), 295–298.
3 M. L. Gardel, K. E. Kasza, C. P. Brangwynne, J. Liu and D. A. Weitz, Mechanical response of cytoskeletal networks, *Methods Cell Biol.*, 2008, **89**, 487–519.
4 N. Y. Yao, D. J. Becker, C. P. Broedersz, M. Depken, F. C. Mackintosh, M. R. Pollak and D. A. Weitz, Nonlinear viscoelasticity of actin transiently cross-linked with mutant -actinin-4, *J. Mol. Biol.*, 2011, **411**, 1062–1071.
5 C. P. Broedersz and F. C. MacKintosh, Molecular motors stiffen non-affine semiflexible polymer networks, *Soft Matter*, 2011, **7**, 3186.
6 P. A. Janmey, M. E. McCormick, S. Rammensee, J. L. Leight, P. C. Georges and F. C. MacKintosh, Negative normal stress in semiflexible biopolymer gels, *Nat. Mater.*, 2007, **6**(1), 48–51.
7 H. Kang, Q. Wen, P. A. Janmey, J. X. Tang, E. Conti and F. C. MacKintosh, Nonlinear elasticity of stiff filament networks: strain stiffening, negative normal stress, and filament alignment in fibrin gels, *J. Phys. Chem. B*, 2009, **113**(12), 3799–805.
8 M. Das, F. C. MacKintosh and A. J. Levine, Effective medium theory of semiflexible filamentous networks, *Phys. Rev. Lett.*, 2007, **99**, 038101.
9 D. A. Head, A. J. Levine and F. C. MacKintosh, Deformation of cross-linked semiflexible polymer networks, *Phys. Rev. Lett.*, 2003, **91**, 108102.
10 D. A. Head, A. J. Levine and F. C. MacKintosh, Distinct regimes of elastic response and deformation modes of cross-linked cytoskeletal and semiflexible polymer networks, *Phys. Rev. E: Stat. Phys., Plasmas, Fluids, Relat. Interdiscip. Top.*, 2003, **68**, 061907.
11 E. Conti and F. C. Mackintosh, Cross-linked networks of stiff filaments exhibit negative normal stress, *Phys. Rev. Lett.*, 2009, **102**, 088102.
12 K. E. Kasza, C. P. Broedersz, G. H. Koenderink, Y. C. Lin, W. Messner, E. A. Millman, F. Nakamura, T. P. Stossel, F. C. Mackintosh and D. A. Weitz, Actin filament length tunes elasticity of flexibly cross-linked actin networks, *Biophys. J.*, 2010, **99**, 1091–1100.
13 J. X. Tang, P. A. Janmey, T. P. Stossel and T. Ito, Thiol oxidation of actin produces dimers that enhance the elasticity of the F-actin network, *Biophys. J.*, 1998, **76**(4), 2208–2215.
14 F. Gittes and F. C. MacKintosh, Dynamic shear modulus of a semiflexible polymer network, *Phys. Rev. E: Stat. Phys., Plasmas, Fluids, Relat. Interdiscip. Top.*, 1998, **58**, R1241.
15 Q. Wen and P. A. Janmey, Polymer physics of the cytoskeleton, *Curr. Opin. Solid State Mater. Sci.*, 2011, **15**, 177–182.
16 P. R. Onck, T. Koeman, T. Van Dillen and E. Van der Giessen, Alternative explanation of stiffening in cross-linked semiflexible networks, *Phys. Rev. Lett.*, 2005, **95**, 178102.
17 J. F. Marko and E. D. Siggia, Stretching D. N. A., *Macromolecules*, 1995, **28**(26), 8759.

18 T. Kim, W. Hwang, H. Lee and R. D. Kamm, Computational analysis of viscoelastic properties of crosslinked actin networks, *PLoS Comput. Biol.*, 2009, **5**, e1000439.
19 M. L. Gardel, J. H. Shin, F. C. MacKintosh, L. Mahadevan, P. A. Matsudaira and D. A. Weitz, Scaling of F-actin network rheology to probe single filament elasticity and dynamics, *Phys. Rev. Lett.*, 2004, **93**, 188102.
20 R. Tharmann, M. M. Claessens and A. R. Bausch, Viscoelasticity of isotropically cross-linked actin networks, *Phys. Rev. Lett.*, 2007, **98**, 088103.
21 M. Arslan and M. C. Boyce, Constitutive modeling of the finite deformation behavior of membranes possessing a triangulated network microstructure, *J. Appl. Mech.*, 2006, **73**(4), 536–543.
22 J. S. Palmer and M. C. Boyce, Constitutive modeling of the stress strain behavior of F-actin filament networks, *Acta Biomater.*, 2008, **4**(3), 597–612.
23 C. P. Brangwynne, F. C. MacKintosh, S. Kumar, N. A. Geisse, J. Talbot, L. Mahadevan, K. K. Parker, D. E. Ingber and D. A. Weitz, Microtubules can bear enhanced compressive loads in living cells because of lateral reinforcement, *J. Cell Biol.*, 2006, **173**(5), 733–741.
24 K. D. Costa, W. J. Hucker and F. C. Yin, Buckling of actin stress fibers: a new wrinkle in the cytoskeletal tapestry, *Cell Motil. Cytoskeleton*, 2002, **52**(4), 266–274.
25 e Silva MS, Depken M, Stuhrmann B, Korsten M, MacKintosh FC, and Koenderink GH. Active multistage coarsening of actin networks driven by myosin motors, *Proc. Natl. Acad. Sci. U. S. A.*, 2011, **108**, 9408–9413.
26 C. Y. Tang, L. C. Zhang and K. Mylvaganamb, Rate dependent deformation of a silicon nanowire under uniaxial compression: yielding, buckling and constitutive description, *Comput. Mater. Sci.*, 2012, **51**, 117.
27 S. Pronk and P. L. Geissler, Faster strain fluctuation methods through partial volume updates, *J. Chem. Phys.*, 2009, **130**, 194706.
28 B. Erman, J. E. Mark. *Structures and Properties of Rubberlike Networks*. Oxford University Press; 1997.
29 T. van Dillen, P. R. Onck and E. Van der Giessen, Models for stiffening in cross-linked biopolymer networks: a comparative study, *J. Mech. Phys. Solids*, 2008, **56**, 2240–2264.
30 M. Bai, A. R. Missel, W. S. Klug and A. J. Levine, The mechanics and affine–nonaffine transition in polydisperse semiflexible networks, *Soft Matter*, 2011, **7**, 907–914.
31 M. Bai, A. R. Missel, A. J. Levine and W. S. Klug, On the role of the filament length distribution in the mechanics of semiflexible networks, *Acta Biomater.*, 2011, **7**, 2109–2118.
32 A. R. Missel, M. Bai, M. S. Klug and A. J. Levine, Affine-nonaffine transition in networks of nematically ordered semiflexible polymers, *Phys. Rev. E: Stat., Nonlinear, Soft Matter Phys.*, 2010, **82**, 041907.
33 P. Chen and V. B. Shenoy, Strain stiffening induced by molecular motors in active crosslinked biopolymer networks, *Soft Matter*, 2011, **7**, 355–358.
34 T. Kreis, R. Vale. *Guidebook to the Cytoskeletal and Motor Proteins.* New York: Oxford University Press; 1999.
35 R. Niederman, P. C. Amrein and J. Hartwig, Three-dimensional structure of actin filaments and of an actin gel made with actin-binding protein, *J. Cell Biol.*, 1983, **96**(5), 1400–1413.
36 Y. Zhang and D. M. Crothers, Statistical mechanics of sequence-dependent circular DNA and its application for DNA cyclization, *Biophys. J.*, 2003, **84**(1), 136–153.
37 T. Su and P. K. Purohit, Thermomechanics of a heterogeneous fluctuating chain, *J. Mech. Phys. Solids*, 2010, **58**(2), 164–186.
38 P. K. Purohit, M. E. Arsenault, Y. E. Goldman and H. H. Bau, The mechanics of short rod-like molecules in tension, *Int. J. Nonlinear Mech.*, 2008, **43**, 1056–1063.
39 T. Su and P. K. Purohit, Fluctuating elastic filaments under distributed loads, *Mol Cell Biomech*, 2011, **8**, 215–232.
40 T. Su, S. K. Das, M. Xiao and P. K. Purohit, Transition between two regimesdescribing internal fluctuation of DNA in a nanochannel, *PLoS One*, 2011, **6**, e16890.
41 M. F. Coughlin, Stamenović DA. A tensegrity model of the cytoskeleton in spread and round cells, *J. Biomech. Eng.*, 1998, **120**, 770–777.
42 Z. P. Bažant, Cedolin Luigi, Stability of structures: elastic, inelastic, fracture, and damage theories, *Courier Dover Publications*, 2003.
43 K. Baczynski, R. Lipowsky and J. Kierfeld, Stretching of buckled filaments by thermal fluctuations, *Phys. Rev. E: Stat., Nonlinear, Soft Matter Phys.*, 2007, **76**, 061914.
44 M. Emanuel, H. Mohrbach, M. Syar and H. Schiessel, Kulić IM. Buckling of stiff polymers: Influence of thermal fluctuations, *Phys. Rev. E: Stat., Nonlinear, Soft Matter Phys.*, 2007, **76**, 061907.
45 N. K. Lee, A. Johner and S. C. Hong, Compressing a rigid filament: Buckling and cyclization, *Eur. Phys. J. E*, 2007, **24**, 229–241.
46 L. J. Gibson, M. F. Ashby *Cellular Solids: Structure and Properties.* Cambridge University Press; 1999.
47 D. H. Boal. *Mechanics of the cell.* Cambridge: Cambridge University Press; 2002.
48 Y. C. Lin, G. H. Koenderink, F. C. MacKintosh and D. A. Weitz, Control of non-linear elasticity in F-actin networks with microtubules, *Soft Matter*, 2011, **7**, 902.
49 E. M. Huisman, C. Heussinger, C. Storm and G. T. Barkema, Semiflexible filamentous composites, *Phys. Rev. Lett.*, 2010, **105**, 118101.

ART ■ C2SM07058H